A Raman study of the organic superconductor κ-(BEDT-TTF)$_2$Cu(SCN)$_2$ at high pressure

2001 J. Phys.: Condens. Matter 13 L291

(http://iopscience.iop.org/0953-8984/13/15/101)

INSTITUTE OF PHYSICS PUBLISHING JOURNAL OF PHYSICS: CONDENSED MATTER

J. Phys.: Condens. Matter **13** (2001) L291–L298 www.iop.org/Journals/cm PII: S0953-8984(01)22578-8

LETTER TO THE EDITOR

A Raman study of the organic superconductor κ-(BEDT-TTF)$_2$Cu(SCN)$_2$ at high pressure

R D McDonald[1], A-K Klehe[1], A P Jephcoat[2], H Olijnyk[2], T Sasaki[3], W Hayes[1], J Singleton[1]

[1] Clarendon Laboratory, Department of Physics, Parks Road, Oxford, OX1 3PU, UK
[2] Department of Earth Sciences, Parks Road, Oxford, OX1 3PR, UK
[3] Institute for Materials Research, Tohoku University, Tohoku, Aoba Ku, Sendai, Miyagi 9808577, Japan

E-mail: r.mcdonald1@physics.ox.ac.uk

Received 6 March 2001

Abstract

The Raman spectrum of the organic superconductor κ-(BEDT-TTF)$_2$Cu(SCN)$_2$ has been measured under hydrostatic pressures up to 1.5 GPa at room temperature. Linear variation of all the observed modes with pressure confirms the absence of a structural phase transition in this pressure range. The Raman spectra reveal three low-frequency features that rapidly stiffen with pressure, $\mathrm{d}\ln\nu/\mathrm{d}P = 5$–17% GPa^{-1}; comparison with x-ray data indicates assignment to lattice modes. By contrast, most Raman-active intramolecular vibrations stiffen by only 0.1–1% GPa^{-1}. Contrary to expectations from a previous high-pressure x-ray study, we do not observe a pressure induced splitting of the $3A_g$ mode.

(Some figures in this article are in colour only in the electronic version; see `www.iop.org`)

Introduction

κ-(BEDT-TTF)$_2$Cu(SCN)$_2$ is one of the best characterized organic molecular metals [1]. This material has a layered structure with polymeric $Cu(SCN)_2^-$ anion planes separating planes of the electron donor molecule BEDT-TTF [bis(ethylenedithio)tetrathiafulvalene], commonly abbreviated to ET. The layers are ionically bound, with pairs of ET molecules jointly donating an electron to the anion layer, leaving a hole in the highest occupied molecular orbital of ET [1]. These dimers stack with alternating orientation in the κ phase structure. The overlap of molecular orbitals thus gives rise to a partially-occupied quasi-two dimensional band structure, which is observed in magnetotransport and de Haas–van Alphen effect measurements [1, 2]. The highly anisotropic structure is also evident in both the optical properties [3] and the compressibility [4].

At ambient pressure κ-(BEDT-TTF)$_2$Cu(SCN)$_2$ is a superconductor with a transition temperature of $T_c \simeq 10.4$ K. This decreases upon the application of pressure until, at pressures P exceeding 0.5 GPa, superconductivity is fully suppressed [2, 5]. Our recent high-pressure infrared study [3] of this material revealed anomalously large mode stiffening for the molecular

vibrations most strongly coupled to the electronic excitations. In this letter we report the the first high-pressure Raman study of this material.

Experiment

Randomly oriented fragments of sample were placed inside a Mao-Bell-type diamond-anvil cell [6] in direct contact with either the top or bottom diamond. The diamonds have 0.8 mm flat culets; these seal the 0.3 mm diameter sample chamber which is drilled into a stainless steel gasket. High-pressure fluid helium was loaded at 0.2 GPa as the pressure transmitting medium [6]; the pressure was adjusted with a mechanical lever mechanism and determined by the ruby fluorescence method [7]. Room temperature Raman spectra were excited by the 514.5 nm line of an Ar^+ ion laser defocussed onto an area of $20 \times 20\ \mu m^2$. A Neon lamp was used to calibrate the spectrometer before and after every measurement and repeated measurement of the ambient pressure ruby line throughout the experiment resulted in a pressure resolution of better than ± 0.02 GPa.

κ-(BEDT-TTF)$_2$Cu(SCN)$_2$ has a low Raman scattering efficiency, but strong optical absorption. Hence, relatively low laser powers easily cause thermal damage to the sample surface. We used the pressure-cell diamond as well as the helium pressure medium as a heatsink to reduce laser heating of the sample. Despite the good thermal contact, the samples were degraded by excessive laser intensity or prolonged weak exposure. The thermal degradation is observed as the irreversible occurrence of a broad hump around 1500 cm^{-1}, consistent with the presence of amorphous carbon [8]. To minimize this effect the laser power was kept at the lowest limit for detectability and a different crystallite was measured for each scan.

The scattered light, collected through a spatial filtering aperture, was analysed at an angle of 135° with respect to the incoming laser beam, using a 0.6 m SPEX triple grating spectrometer and a liquid-nitrogen-cooled, back illuminated, CCD multichannel detector. The spectrum was collected in four sections 50–740 cm^{-1}, 570–1220 cm^{-1}, 1170–1750 cm^{-1} and 1670–2250 cm^{-1}, each section requiring a two hour exposure, as a result of the low incident power. The peak position uncertainties are due to the line widths and the signal-to-noise ratio, not the absolute resolution of the spectrometer ($\sim$0.1 cm^{-1}). No data could be obtained in the region 1240–1365 cm^{-1} due to the presence of the strong first-order diamond phonon mode of the low fluorescence diamond-anvil.

Results

Figure 1 shows the room-temperature Raman spectrum of κ-(BEDT-TTF)$_2$Cu(SCN)$_2$ obtained at 0.3 GPa. The observed features, listed in table 1, can be separated into two groups: the intramolecular vibrations, identified according to previous mode assignment [9], and lattice vibrations at low frequencies.

The strong pressure dependence of the three modes at 60, 96 and 131 cm^{-1} suggests that they are lattice vibrations. The 96 and 131 cm^{-1} modes have been previously observed [9] but not conclusively assigned. The lowest-frequency mode is only resolved at pressures exceeding 0.8 GPa, when it emerges from the broad sample fluorescence around the laser line. This association is supported by comparison of the ratio of the first order frequency shifts $\mathrm{d}\ln\nu/\mathrm{d}P$ extracted from figure 2 with the linear compressibility ratios for the three crystal axes [4]:

$$\frac{\mathrm{d}\ln\nu_3}{\mathrm{d}P} : \frac{\mathrm{d}\ln\nu_2}{\mathrm{d}P} : \frac{\mathrm{d}\ln\nu_1}{\mathrm{d}P} = 1 : 2.8 : 3.1 \tag{1}$$

$$\kappa_a : \kappa_b : \kappa_c = 1 : 2.5 : 3.6. \tag{2}$$

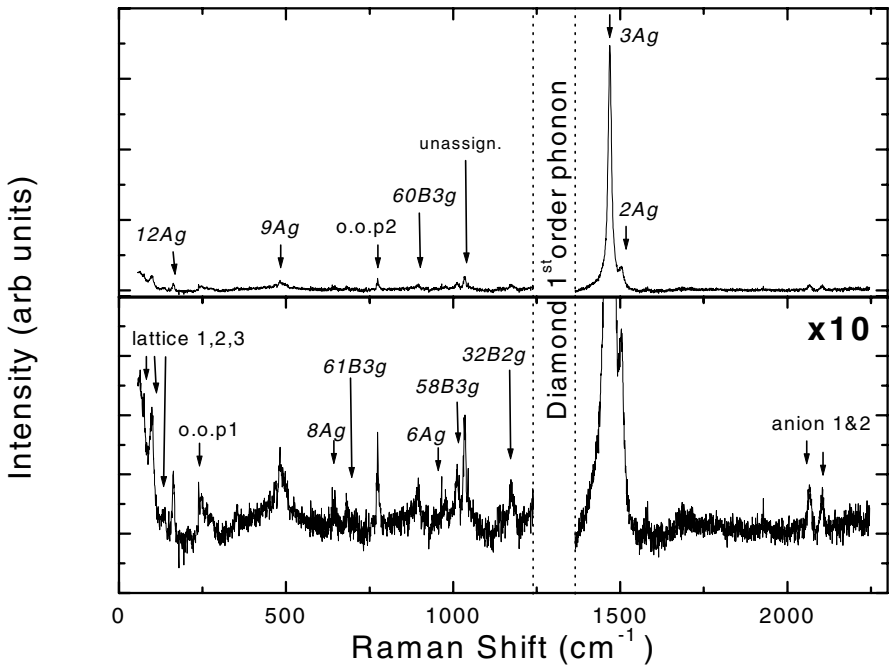

Figure 1. A typical room temperature Raman spectrum obtained at 0.3 GPa (excitation: 514.532 nm).

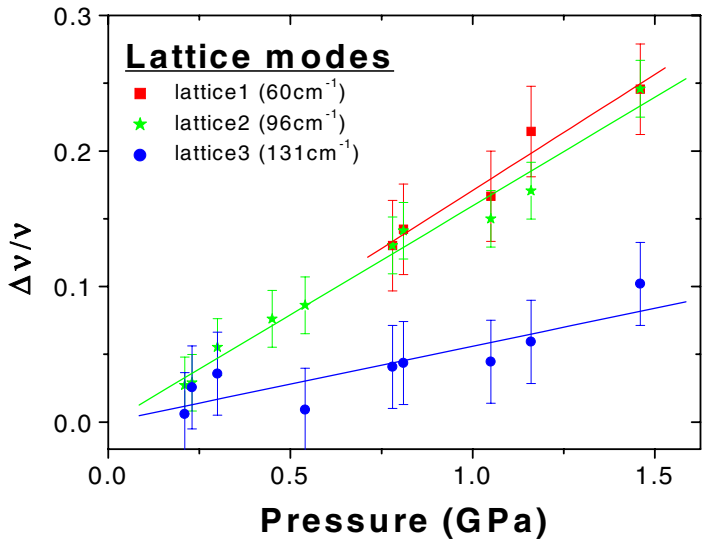

Figure 2. The pressure-induced frequency shifts at room temperature of the three low frequency lattice modes are 17.1 %GPa^{-1} for mode 1, 15.8 %GPa^{-1} for mode 2 and 5.59 %GPa^{-1} for mode 3.

The similar pressure dependence of modes 1 and 2 (see figure 2) reflect the similarity of the crystallographic *b* and *c* axes [4], indicating that these modes most likely propagate in the *bc* plane. Mode 3 is associated with the interplane direction; the relatively high frequency

Table 1. Mode assignments and first-order pressure shifts extracted from figures 2 and 3.

Mode assignment	Linear extrapolation to ambient pressure Raman shift (cm^{-1})	First-order pressure shift (% GPa^{-1})
Lattice 1	59.9 ± 1.4	17.1 ± 2.23
Lattice 2	95.5 ± 0.8	15.8 ± 1.08
Lattice 3	130.5 ± 1.3	5.59 ± 1.23
12 A_g	162.0 ± 0.4	2.51 ± 0.33
Out of plane 1	245.5 ± 0.5	1.92 ± 0.39
9 A_g	500.0 ± 2.0	——
8 A_g	641.9 ± 0.5	0.715 ± 0.073
61 $B3_g$	680.1 ± 0.8	0.600 ± 0.121
Out of plane 2	774.1 ± 0.1	0.136 ± 0.020
60 $B3_g$	886.2 ± 0.6	0.854 ± 0.070
6 A_g	977.4 ± 0.2	-0.176 ± 0.023
58 $B3_g$	1009.0 ± 0.3	0.278 ± 0.042
Unassign	1032.9 ± 0.3	0.294 ± 0.036
32 $B2_g$	1175.8 ± 1.5	0.845 ± 0.148
3 A_g	1467.7 ± 0.3	0.393 ± 0.024
2 A_g	1503.0 ± 2.0	——
Anion 1	2064.6 ± 0.4	0.136 ± 0.024
Anion 2	2106.3 ± 0.3	0.160 ± 0.017

compared to modes 1 and 2 is consistent with this mode involving both the layers of ET molecules and the relatively light anion planes.

X-ray scattering experiments [4] indicate that compression of the unit cell mainly results from reduction of the intermolecular distances, rather than distortion or compression of the molecules themselves. Therefore, having made the association of the low-frequency modes with lattice vibrations, we calculated the lattice Grüneisen parameters, γ_i [10], from the uniaxial compressibility, κ_i [4], and our frequency shifts:

$$\gamma_i = \frac{1}{3\kappa_i}\frac{\mathrm{d}\ln \nu_i}{\mathrm{d}P}. \tag{3}$$

The values obtained, $\gamma_1 = 1.6$, $\gamma_2 = 2.1$ and $\gamma_3 = 1.8$, are typical for ionically-bonded solids [10, 11]. These Grüneisen parameters can be taken as further evidence for the correct assignment of these modes as lattice modes.

The pressure dependences of the intramolecular ET and anion modes are shown in figure 3; they have a pressure dependence of 0.1–1% GPa^{-1}, much smaller than that of the lattice modes. Features in the frequency regions around 250 cm^{-1} and 500 cm^{-1} are characterized by a dense collection of Raman active modes [12]. Their pressure dependence could not be resolved unambiguously in this experiment throughout the whole pressure range.

The Grüneisen parameters for the internal (intramolecular) modes of molecular crystals are known to deviate from the frequency-independent parameters expected in simple network crystals [13]. This is because the *intra*molecular bonds provide the greater part of the restoring forces for the vibrations, whilst it is chiefly the *inter*molecular bonds that change length due to the pressure-induced compression. Nevertheless, it is useful to display the intramolecular Grüneisen parameters to further highlight the difference between the inter- and intramolecular modes. Figure 4 shows how the Grüneisen parameters γ_j, defined by

$$\gamma_j = \frac{1}{\kappa_{\mathrm{vol}}}\frac{\mathrm{d}\ln \nu_j}{\mathrm{d}P} \tag{4}$$

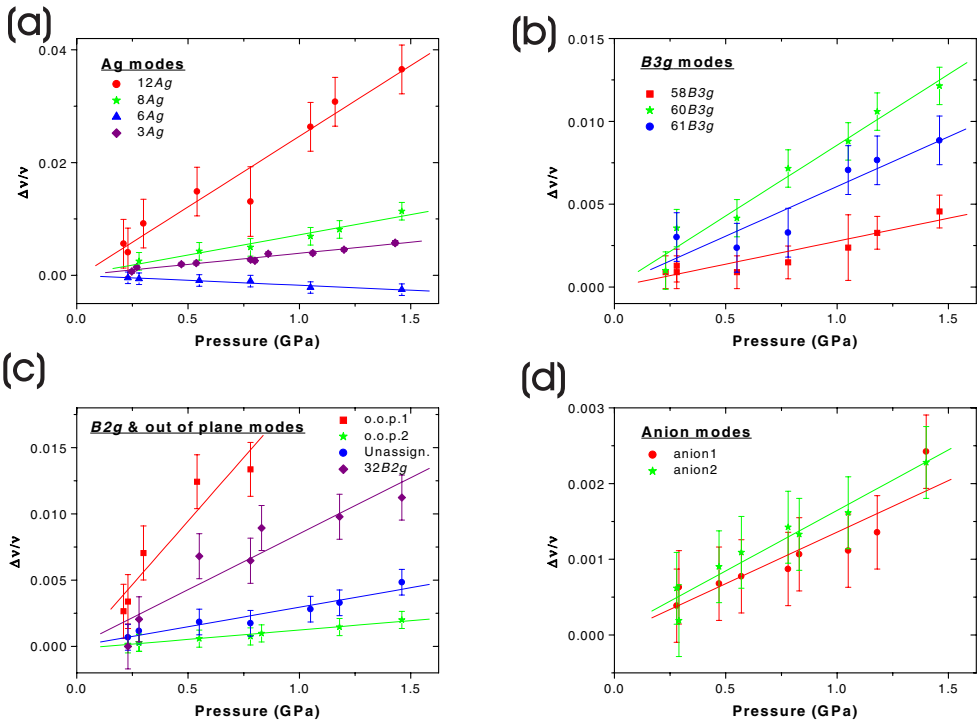

Figure 3. The pressure induced frequency shifts at room temperature of the (a) A_g modes (b) $B3_g$ modes (c) out of plane, $B2_g$ and unassigned modes of the ET molecule; (d) anion modes.

depend on mode frequency. It should be noted that we differentiate between the volume-compressibility, $\kappa_{\rm vol}$, definition used in equation (4) and the uniaxial definition (used for the lattice modes) in equation (3) by use of subscripts i and j. The former indicates a crystallographic direction, whilst the latter indexes a particular mode.

Following work on molecular sulphur crystals [13], where the Grüneisen parameters span several orders of magnitude, it was proposed that a general scaling relation of ν^{-2} exists for molecular crystals. The Grüneisen parameters calculated here (see figure 4) similarly span several orders of magnitude, but appear more scattered and obey a power law closer to ν^{-1}.

Using the normal mode coordinate analysis for neutral ET [14], we attempted to find a correlation between the pressure coefficient of the intramolecular mode frequencies and the atomic displacement vectors for each mode but had limited success. For example, using the a axis compressibility the Grüneisen parameter for the intramolecular mode with the highest pressure coefficient ($12A_g$) (see table 1) is 0.8. Examination of the normal molecular mode displacement vectors [14] indicates that the $12A_g$ mode is predominantly a symmetric stretching of the four inner C–S bonds along the a axis, with the ends of the molecule moving into the space between the ET and the anion planes, whereas the stiffer modes, with smaller Grüneisen parameters, increasingly involve internal displacement of atoms as expected. However, both the $6A_g$ and $60B3_g$ modes are predominantly stretch modes of the C–S bonds along the edge of the ET molecule. The $60B3_g$ mode stiffens by 0.85% GPa^{-1} whereas the $6A_g$ mode is the only mode to soften, -0.17% GPa^{-1}, an observation we cannot account for at this time.

As in previous studies [9, 14], the spectrum's dominant feature is attributed to the $3A_g$

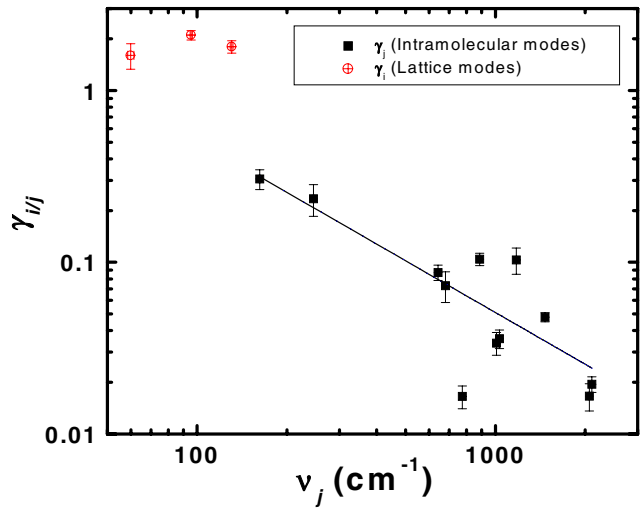

Figure 4. The dependence of Grüneisen parameter on mode frequency.

intramolecular mode. The $2A_g$ and $3A_g$ modes in neutral ET are predominently the central double bond oscillating in and out of phase respectively with the ring double carbon bonds.

Polarization studies [15] and the absence of $2A_g$ around 1551 cm^{-1} [9] indicate a deviation from the normal modes observed in the neutral ET molecule. Within the structure of κ-(BEDT-TTF)$_2$Cu(SCN)$_2$ the observable normal modes are much closer in frequency and their relative intensities are strongly dependent on the crystal axis [15]. This implies limited mixing of the central and ring double bond oscillations. The $3A_g$ feature is strongest with the excitation polarisation in the interplane direction, indicating that it is associated with the central double bond and the shoulder, around 1503 cm^{-1}, with the ring double bond. This association of the $2A_g$ and $3A_g$ modes with particular bonds suggests that Badger's rules [16], emperically determined proportionality constants linking force constant and bond length for simple molecular species, may be employed. This enables an approximation of the central C=C mode softening or stiffening to be made given the bond length change with pressure [4]. To compare this change in force constant to the observed pressure-induced frequency shift, we employ a dynamical matrix approach [17] to model the coupled molecular vibrations.

The inclusion of intermolecular vibrational coupling produces a weakly dispersive optic phonon branch for each molecular vibration. Dimerization, i.e. two different intermolecular force constants, is a necessary condition for in-plane optical lattice phonons in this material. This causes a Davydov-type splitting [13] of the intramolecular modes: the weakly dispersive band folded back on itself. In the long-wavelength limit this is equivalent to replacing the D_{2h} symmetry group of the individual molecules with C_{2h} for the dimer pair [18, 19], doubling the number of modes in the process. The frequency splitting at the zone centre, $\omega_{\rm split}$, is independent of the lattice mode dispersion, depending only on its optic branch frequency at the zone centre, $\omega_{\rm lattice}$,

$$\omega_{\rm split} = \frac{\omega_{\rm lattice}^2}{2\,\omega_{\rm mol}} \tag{5}$$

where $\omega_{\rm mol}$ is the frequency of the uncoupled intramolecular mode. With identical molecules at each dimer site the atomic displacement vectors calculated using a dynamical matrix approach reveal the split modes to be symmetric and asymmetric (in-phase and anti-phase) combinations

of the molecular modes. It has been shown [19] using the C_{2h} symmetry group to represent an isolated dimer, that the D_{2h} group's 12 A_g modes split into 24 modes. The symmetric combinations remain A_g Raman active modes and the asymmetric combinations become infrared active B_u modes, i.e. we only measure the symmetric combination.

The high-pressure x-ray data suggest that the central C=C bond shortens in one of the molecules of the dimer (1.37–1.31 Å) and lengthens in the other (1.37–1.40 Å) between ambient pressure and 0.75 GPa [4]. In order to test whether this indeed happens, we convert the suggested length changes to fractional force constant changes via Badger's rules; re-calculation of displacement vectors allows examination of the evolution of mode symmetry with pressure. With the suggested bond changes, the symmetric combination evolves towards a mode dominated by the softer of the two molecules and the asymmetric combination towards a mode dominated by the stiffer molecule, breaking the C_{2h} symmetry in the process; i.e. both modes regain their Raman activity. However, we find no evidence for this splitting of the $3A_g$ mode with pressure (see figure 5) casting considerable doubt on the refinement method employed in the x-ray study [4].

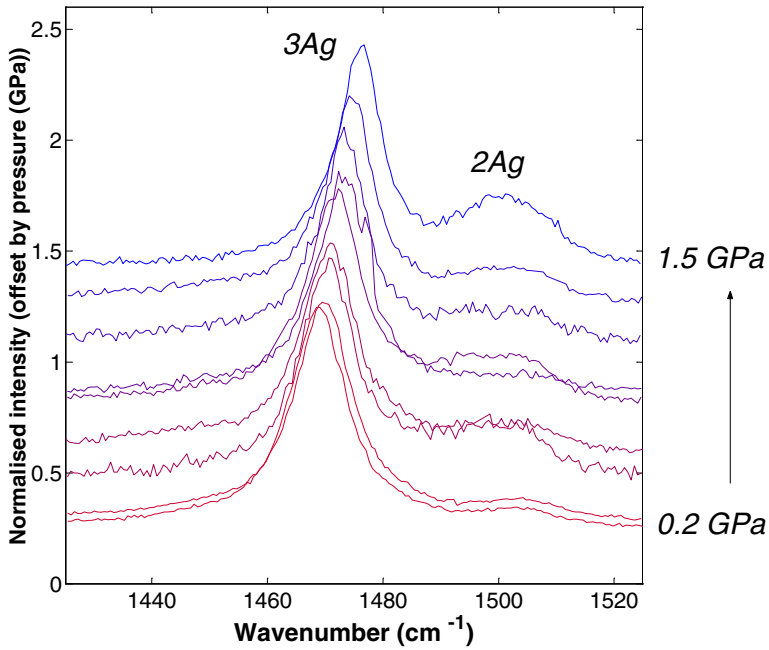

Figure 5. Spectral region containing the $2A_g$ and $3A_g$ modes. Raman intensities have been normalized and offset by pressure for clarity.

The splitting of the $3A_g$ mode with temperature in the spectrum of other ET salts is used as a measure of the dimer's charge distribution [20]. Splitting of this mode is usually associated with a metal-insulator transition; i.e. the charge redistribution associated with the differential bond length change tends to cause electron localization [20]. The absence of splitting of the $3A_g$ mode in the Raman spectrum with pressure indicates the absence of a differential length change of the two molecules in the dimer. This implies a constant charge distribution, consistent with hydrostatic pressure increasing the metallic nature of the sample [2, 5].

The line shape of the shoulder labelled $2A_g$ in figure 5, indicates the possibility of an unresolved doublet, but a reliable pressure trend could not be extracted. This is possibly due

to the varying background in this spectral region, which was found to correlate with thermal degradation of the sample.

Conclusions

In summary, we have studied the Raman spectrum of the organic superconductor κ-(BEDT-TTF)$_2$Cu(SCN)$_2$ under hydrostatic pressures of up to 1.5 GPa at room temperature. No structural phase transitions could be detected up to 1.5 GPa. The Raman spectra reveal three low-frequency features that rapidly stiffen with pressure, $\mathrm{d}\ln\nu/\mathrm{d}P = 5$–$17\%$ GPa^{-1}; the calculation of Grüneisen parameters enables these features to be identified as lattice modes. In contrast, most Raman-active intramolecular vibrations stiffen by only 0.1–1% GPa^{-1}. The absence of a pressure-induced splitting of the $3A_g$ mode suggests that the refinement method used in previous high-pressure x-ray analysis was inadequate.

References

[1] Singleton J 2000 *Rep. Prog. Phys.* **63** 1111
[2] Caulfield J, Lubcynski W, Lee W, Singelton J, Pratt F L, Hayes W, Kurmoo M and Day P 1995 *Synth. Metals* **70** 185
[3] Klehe A-K, McDonald R D, Goncharov A F, Struzhkin V V, Mao H, Hemley R J, Sasaki T, Hayes W and Singleton J 2000 *J. Phys.: Condens. Matter* **12** L247
[4] Rahal M, Chasseau D, Gaultier J, Ducasse L, Kurmoo M and Day P 1997 *Acta Cryst.* B **53** 159
[5] Murata K, Honda Y, Anxai H, Tokumoto M, Takahashi K, Kinshita N and Ishiguro T 1989 *Synth. Metals* **27** A263
[6] Jephcoat A P, Mao H-K and Bell P M 1987 *Hydrothermal Experimental Techniques* G C Ulmer and H L Barnes (ed) (New York: Wiley p 469
[7] Mao H K, Xu J and Bell P M 1986 *J. Geophys. Res.* **91** 4673
[8] Chhowalla M, Ferrari A C, Robertson J and Amaratunga G A J 2000 *App. Phys. Lett.* **76** 1419
[9] Eldridge J E, Xie Y, Lin Y, Homes C C, Wang H H, Williams J M, Kini A M and Schlueter J A 1997 *Spectrochim. Acta* A **53** 565
[10] Sherman W F 1980 *J. Phys. C : Solid St. Phys* **13** 4601
[11] White G C *Proc. R. Soc. London* A **286** 204
[12] Lin Y, Eldridge J E, Wang H H, Kini A M, Kelly E M, Williams J M and Schlueter J A 1999 *Synth. Metals* **103** 2071
[13] Zallen R 1974 *Phys. Rev.* B **9** 4485
[14] Eldridge J E, Xie Y, Wang H H, Williams J M, Kini A M and Schlueter J A 1996 *Spectrochim. Acta* A **52** 45
[15] Bowman P 1994 *DPhil thesis* University of Oxford
[16] Badger R M 1934 *J. Chem. Phys.* **2** 128
[17] Dove M T 1993 *Introduction to Lattice Dynamics* (Cambridge: Cambridge University Press)
[18] Eldridge J E, Homes C C, Williams J M, Kini A M and Wang H H 1995 *Spectrochim. Acta* A **51A** 947
[19] Kozlov M E and Tokumoto M 1995 *Synth. Metals* **70** 1023
[20] Inokuchi M, Yakushi K, Kinoshita M and Saito G 1999 *Synth. Metals* **103** 2001